



OPEN

## S-SCAM inhibits Axin-dependent synaptic function of GSK3 $\beta$ in a sex-dependent manner

Gillian Kearney<sup>1</sup>, David Grau<sup>1</sup>, Damaris Nieves Torres<sup>1</sup>, Seung Min Shin<sup>1</sup> & Sang H. Lee<sup>1,2</sup>✉

*S-SCAM/MAGI-2* gene duplication is associated with schizophrenia (SCZ). *S-SCAM* overexpression in the forebrain induces SCZ-like phenotypes in a transgenic (Tg) mouse model. Interestingly, *S-SCAM* Tg mice show male-specific impairments in synaptic plasticity and working memory. However, mechanisms underlying the sex-specific deficits remain unknown. Here we report that *S-SCAM* Tg mice have male-specific deficits in synaptic GSK3 $\beta$  functions, as shown by reduced synaptic protein levels and increased inhibitory phosphorylation of GSK3 $\beta$ . This GSK3 $\beta$  hyper-phosphorylation was associated with increased CaMKII activities. Notably, synaptic levels of Axin1, to which GSK3 $\beta$  binds in competition with *S-SCAM*, were also reduced in male *S-SCAM* Tg mice. We demonstrated that Axin-binding is required for the *S-SCAM* overexpression-induced synaptic GSK3 $\beta$  reduction. Axin stabilization using XAV939 rescued the GSK3 $\beta$  deficits and restored the temporal activation of GSK3 $\beta$  during long-term depression in *S-SCAM* overexpressing neurons. Interestingly, synaptic Axin2 levels were increased in female *S-SCAM* Tg mice. Female sex hormone 17 $\beta$ -estradiol increased Axin2 expression and increased synaptic GSK3 $\beta$  levels in *S-SCAM* overexpressing neurons. These results reveal the role of *S-SCAM* in controlling Axin-dependent synaptic localization of GSK3 $\beta$ . Moreover, our studies point out the pathological relevance of GSK3 $\beta$  hypofunction found in humans and contribute to understanding the molecular underpinnings of sex differences in SCZ.

Synaptic scaffolding molecule (*S-SCAM*; also called membrane-associated guanylate kinase inverted 2 [*MAGI-2*]) is one of the major postsynaptic scaffolding molecules present at synapses<sup>1–4</sup>. *S-SCAM* interacts with many postsynaptic proteins including Axin, transmembrane AMPA receptor regulatory protein (TARP), and GKAP/SAPAP<sup>5–7</sup>. *S-SCAM* dictates the strength of excitatory synaptic transmission by controlling the amounts of AMPA receptors (AMPA) at synapses through its TARP interaction<sup>1,5,8</sup>. Importantly, mutations in the *S-SCAM* gene including duplication are found in patients with SCZ<sup>9–12</sup>. Mimicking the duplication conditions, *S-SCAM* overexpression in cultured hippocampal neurons enhanced excitatory synaptic transmission<sup>1</sup>, impaired GABAergic synaptic transmission<sup>13</sup>, and impaired synaptic plasticity<sup>1,14</sup>. Therefore, it was expected that elevated *S-SCAM* levels lead to deficits in cognitive function and behavioral abnormalities. Indeed, *S-SCAM* Tg mice that overexpress *S-SCAM* under the forebrain-specific Ca<sup>2+</sup>-dependent protein kinase II a (CaMKIIa) promoter showed a remarkably wide array of SCZ-related behavioral endophenotypes modeling all three domains (positive, negative, and cognitive) of SCZ symptoms<sup>14</sup>. Notably, the *S-SCAM* Tg mice showed interesting sex differences. Male Tg mice showed more severe SCZ-related endophenotypes than female Tg mice. Moreover, only male *S-SCAM* Tg mice showed deficits in long-term potentiation (LTP). These findings are, in general, consistent with the sex differences observed in SCZ<sup>15</sup>. However, the molecular and physiological bases of the sex differences in SCZ are still poorly understood.

Precise temporal control of GSK3 activity is crucial for the induction of LTP and long term depression (LTD)<sup>7,16–18</sup>. GSK3 is encoded by two genes producing GSK3 $\alpha$  and GSK3 $\beta$  isoforms that have similar catalytic activity. GSK3 $\beta$  is the major isoform expressed in the brain<sup>19</sup> and is present in dendritic spines in addition to the soma and dendrites of neurons<sup>17</sup>. GSK3 is constitutively active but the phosphorylation of its Ser residue (pS9 for GSK3 $\beta$ ; pS21 for GSK3 $\alpha$ ) inactivates the kinase<sup>19,20</sup>. During LTD, GSK3 $\beta$  is activated by PP1-mediated de-phosphorylation of pS9. Activated GSK3 $\beta$  phosphorylates Thr19 of PSD-95 to promote the immobilization of PSD-95 at the synapse, which is a prerequisite for AMPA receptor internalization during LTD<sup>21</sup>. On the other hand, the inactivation of GSK3 $\beta$  is required for LTP formation<sup>16,17</sup>.

<sup>1</sup>Department of Pharmacology and Toxicology, Medical College of Wisconsin, 8701 Watertown Plank Road, Milwaukee, WI, USA. <sup>2</sup>Neuroscience Research Center, Medical College of Wisconsin, 8701 Watertown Plank Road, Milwaukee, WI, USA. ✉email: shlee@mcw.edu

Axin is a critical scaffolding protein for forming the GSK3 $\beta$ - $\beta$ -catenin destruction complex in the canonical Wnt signaling<sup>22</sup>. Axin is encoded by two genes producing highly homologous proteins, Axin1 and Axin2 (also known as Axil/conductin)<sup>23</sup>. Axin is enriched at dendritic spines<sup>7,24</sup> and is important for the axonal localization of GSK3 $\beta$  in developing neurons<sup>25,26</sup>. S-SCAM binds to the middle region of Axin1 protein (containing GSK3 $\beta$ -interacting domain [GID]) through its guanylate kinase (GK) domain<sup>7</sup>. The GIDs of Axin1 and Axin2 are highly conserved (~70% similarity at the amino acid sequence level). Since S-SCAM and GSK3 $\beta$  bind the same region in Axin, S-SCAM was shown to compete with GSK3 $\beta$  for Axin-binding<sup>7,26</sup>. This competitive binding inhibits  $\beta$ -catenin phosphorylation by GSK3 $\beta$  in vitro<sup>7</sup>. Therefore, it is likely that GSK3 $\beta$  interaction with Axin is hampered in S-SCAM Tg mice, which may disrupt the proper synaptic localization of GSK3 $\beta$  in neurons. However, these possibilities have not been addressed.

As a first step to understand the molecular bases of the sex differences exhibited in S-SCAM Tg mice, we investigated whether aberrant GSK3 $\beta$  signaling is associated with these phenotypes, as well as the potential role of Axin and female sex hormone in the process. These studies reveal the role of Axin in maintaining proper GSK3 $\beta$  signaling at synapses and provide mechanisms underlying the sex differences found in S-SCAM Tg mice.

## Results

**Synapse-specific reduction of GSK3 $\beta$  protein levels and its activity in male S-SCAM Tg mice.** To study the role of S-SCAM in GSK3 $\beta$ -mediated signaling at synapses (Fig. 1a), we first examined GSK3 $\beta$  protein levels in synaptosomal fractions (P2; biochemical correlates of synapses<sup>27</sup>) of the forebrain tissues obtained from male Tg mice (Tg-M; 3  $\pm$  0.5-month-old). GSK3 $\beta$  protein levels in P2 fractions were greatly reduced (66.7%  $\pm$  4.3% of WT; Fig. 1b, c). On the other hand, GSK3 $\beta$  levels in total homogenate fraction (H) of male Tg mice show no difference from male WT mice (Fig. 1b, d), suggesting that the reduced synaptic GSK3 $\beta$  protein levels are unlikely due to the decreased expression of GSK3 $\beta$ . This synaptic GSK3 $\beta$  reduction is accompanied by increased synaptosomal phospho-Ser9-GSK3 $\beta$  (pS9-GSK3 $\beta$ ) levels (normalized to GSK3 $\beta$  levels; 165.9%  $\pm$  11.4% of WT; Fig. 1e, f). In contrast, pS9-GSK3 $\beta$  levels in total homogenate (H) of male Tg mice showed no difference from male WT mice (Fig. 1e, g). These results suggest that S-SCAM overexpression inhibits synaptic targeting of GSK3 $\beta$  and impairs synaptic GSK3 $\beta$  activity in the brain of male S-SCAM Tg mice.

**Elevated CaMKII activity in the brains of male S-SCAM Tg mice.** To investigate the mechanisms associated with the enhanced inhibitory phosphorylation of synaptic GSK3 $\beta$  in the brains of male S-SCAM Tg mice, we examined the activity of two known upstream protein kinases of GSK3 $\beta$ , CaMKII and Akt<sup>19,28</sup>. Activation of these kinases were assessed by specific antibodies recognizing phosphorylated (and thus activated) forms of CaMKIIa and CaMKIIb (pThr286 and pThr287 for CaMKIIa and CaMKIIb, respectively) and Akt (pSer473). We found that total pCaMKII levels were significantly increased in both P2 and H fractions of male Tg mice (168%  $\pm$  13.6% and 188%  $\pm$  8.6% of WT, respectively; Fig. 2a–c). On the other hand, both pAkt and Akt protein levels were not significantly changed in either P2 or H fractions (Fig. 2a–c). These results suggest that elevation of inhibitory phosphorylation of GSK3 $\beta$  is most likely caused by increased CaMKII activity in male S-SCAM Tg mice. These data are consistent with elevated glutamatergic activity at the synapse found in S-SCAM Tg mice<sup>14</sup>.

**Reduced synaptic GSK3 $\beta$  protein levels in male S-SCAM Tg mice is associated with decreased synaptic Axin1 levels.** Axin1 is one of the S-SCAM-interacting proteins and is known to be involved in the recruitment of GSK3 $\beta$  to the plasma membrane<sup>29</sup>. To investigate the potential role of Axin in the altered synaptic localization of GSK3 $\beta$  in male S-SCAM Tg mice, we first explored the possibility that Axin protein levels are altered in the S-SCAM Tg mice. We examined both Axin1 and Axin2 proteins, since they can be functionally interchangeable<sup>23</sup>. Total protein levels of both Axin1 and Axin2 in the forebrain tissues of male Tg mice were indistinguishable from male WT mice (Fig. 3a, b). In contrast, Axin1 protein levels in the P2 fraction were significantly reduced in male S-SCAM Tg mice (66%  $\pm$  4.2% of WT; Fig. 3a, b). On the other hand, there was no such difference in Axin2 protein levels in the P2 fraction (Fig. 3a, c). Therefore, male S-SCAM Tg mice have Axin1 deficits in synapses of the forebrain.

S-SCAM and GSK3 $\beta$  competitively bind the same region in Axin<sup>7</sup>. Therefore, S-SCAM overexpression may hamper the Axin-mediated synaptic targeting of GSK3 $\beta$ . To address this possibility, we took advantage of the fact that Axin binds to the GK domain of S-SCAM<sup>7</sup>. Therefore, a S-SCAM mutant lacking the GK domain (DGK)<sup>13</sup> should not interfere with the Axin- GSK3 $\beta$  interaction. The DGK mutant is indistinguishable from WT S-SCAM in synaptic targeting, as well as its ability to increase spine sizes and synaptic AMPA receptor levels<sup>13</sup>. Consistent with our hypothesis, while the overexpression of WT S-SCAM greatly reduced synaptic GSK3 $\beta$  levels (59.7%  $\pm$  6% of GFP control; Fig. 3d, e), the overexpression of DGK mutant did not hamper the synaptic targeting of GSK3 $\beta$  (127%  $\pm$  15.2%; Fig. 3d, e). These results strongly suggest S-SCAM overexpression inhibits Axin-mediated synaptic targeting of GSK3 $\beta$ .

**Stabilization of Axin1 restores synaptic targeting and temporal regulation of GSK3 $\beta$  activity during LTD.** To further study the role of Axin1 deficits in the impairment of GSK3 $\beta$  function at synapses, we thought to rescue the deficits using pharmacological approaches. A small molecule tankyrase inhibitor XAV939 stabilizes Axin by preventing ADP-ribosylation and subsequent degradation<sup>30,31</sup>. Incubation of cultured hippocampal neurons transfected with GFP-expressing Sindbis virus with XAV939 (5 mM) for 24 h greatly increased the total amount of Axin1 (171.3%  $\pm$  21% of GFP control; Fig. 4a, b). Total Axin1 levels in cultured hippocampal neurons infected with Sindbis virus overexpressing S-SCAM (Supplementary Fig. 1) were reduced (63.1%  $\pm$  9% of GFP control), although the reduction was not statistically significant ( $p = 0.4462$ ). Nonetheless, XAV939 significantly increased the amount of total Axin1 in S-SCAM overexpressing cultured hippocampal

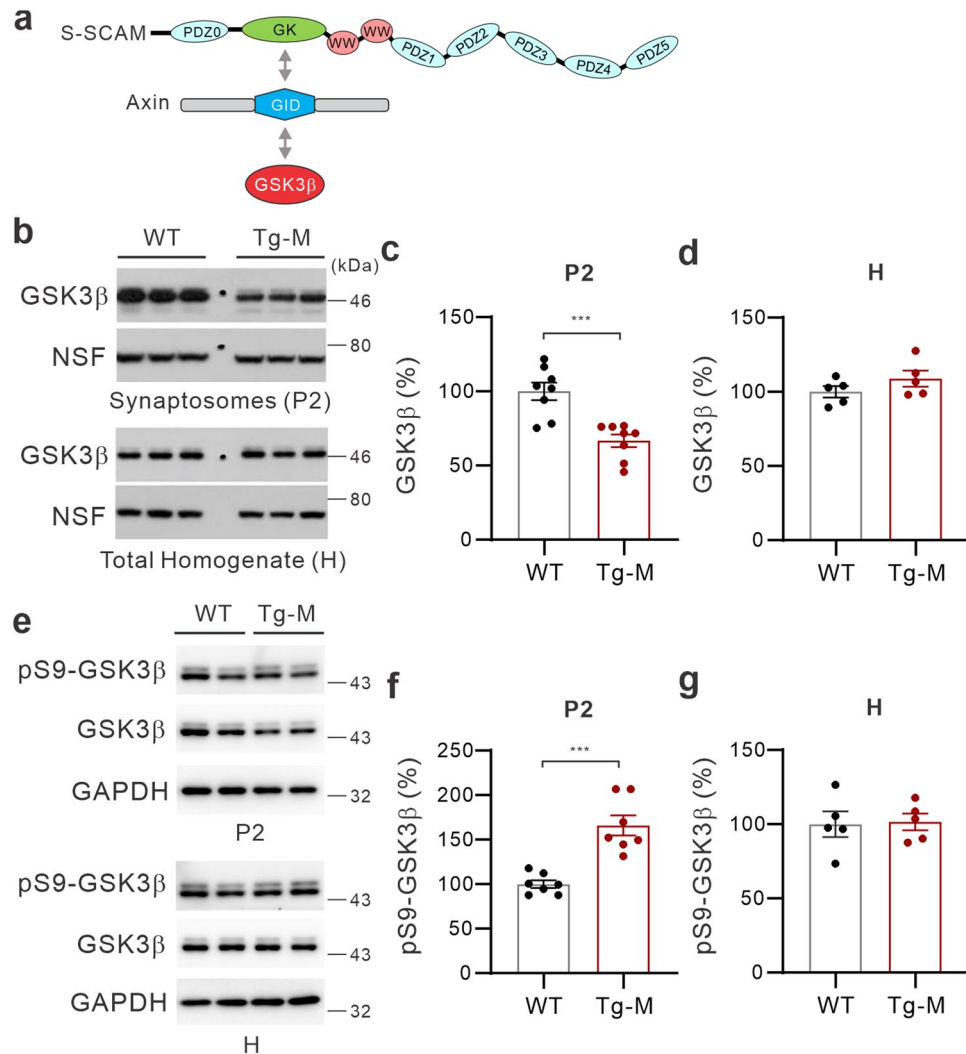


**Figure 1.** Reduced synaptic GSK3 $\beta$  protein levels and hyper-phosphorylation of GSK3 $\beta$  in the forebrain tissues of 3-month-old male S-SCAM Tg mice. **(a)** Schematic diagram showing the competitive binding ( $\leftrightarrow$ ) of S-SCAM with GSK3 $\beta$  for the GID domain of Axin. **(b–d)** GSK3 $\beta$  protein levels in the synaptosomal fraction (P2) and total homogenate (H) of male S-SCAM Tg mice. Representative results **(b)** and quantification **(c, d)**.  $n = 5–8$  mice per group. *N*-ethylmaleimide-sensitive factor (NSF) was used as loading control. **(e–g)** pS9-GSK3 $\beta$  protein levels in the P2 and H fractions. Representative results **(e)** and quantification of relative pS9-GSK3 $\beta$  levels normalized to GSK3 $\beta$  protein levels **(f, g)**.  $n = 5–7$  mice per group. \*\*\* $p < 0.001$ , unpaired *t*-test with Welch's correction. n.s., not significant.

neurons ( $186\% \pm 39\%$  of S-SCAM control;  $117.4\% \pm 25\%$  of GFP control; Fig. 4a, b). Unexpectedly, we did not see significant changes in the amount of total Axin2 after XAV939 treatment in both GFP and S-SCAM overexpressing neurons (Fig. 4a, c).

Having verified the restoration of Axin1 levels in S-SCAM overexpressing neurons, we next examined the effect of XAV939 on synaptic GSK3 $\beta$  levels in S-SCAM overexpressing neurons. Incubation of hippocampal neurons with XAV939 greatly increased synaptic GSK3 $\beta$  staining intensity ( $178\% \pm 19\%$  of GFP control; cf.  $62\% \pm 5\%$  for S-SCAM control; Fig. 4d, e), indicating increased synaptic GSK3 $\beta$  protein levels. In contrast, XAV939 did not change synaptic GSK3 $\beta$  levels in GFP-transfected neurons (Supplemental Fig. 2).

We showed previously that the overexpression of S-SCAM blocks LTD formation in both cultured hippocampal neurons and hippocampal slices<sup>1</sup>. To evaluate the restoration effect of Axin1 and GSK3 $\beta$  protein levels at synapses on synaptic plasticity, we examined the temporal changes of GSK3 $\beta$  activity during LTD which is critical for LTD formation<sup>19</sup>. We used a chemically (NMDA)-induced LTD (chem-LTD) protocol, which mimics the low frequency stimulation-induced LTD mechanistically<sup>21,32</sup>. We first examined whether XAV939 by itself had an effect on GSK3 $\beta$  activation during LTD. XAV939 alone did not affect NMDA-induced activation of GSK3 $\beta$  in GFP overexpressing neurons, as shown by the rapid reduction in the inhibitory phosphorylation of S9 (Fig. 4f, g). This is similar in temporal profile to GFP control and to previous reports obtained from naïve hippocampal neurons<sup>17,21,33</sup>. Having confirmed that XAV939 does not affect the rapid activation of GSK3 $\beta$  upon

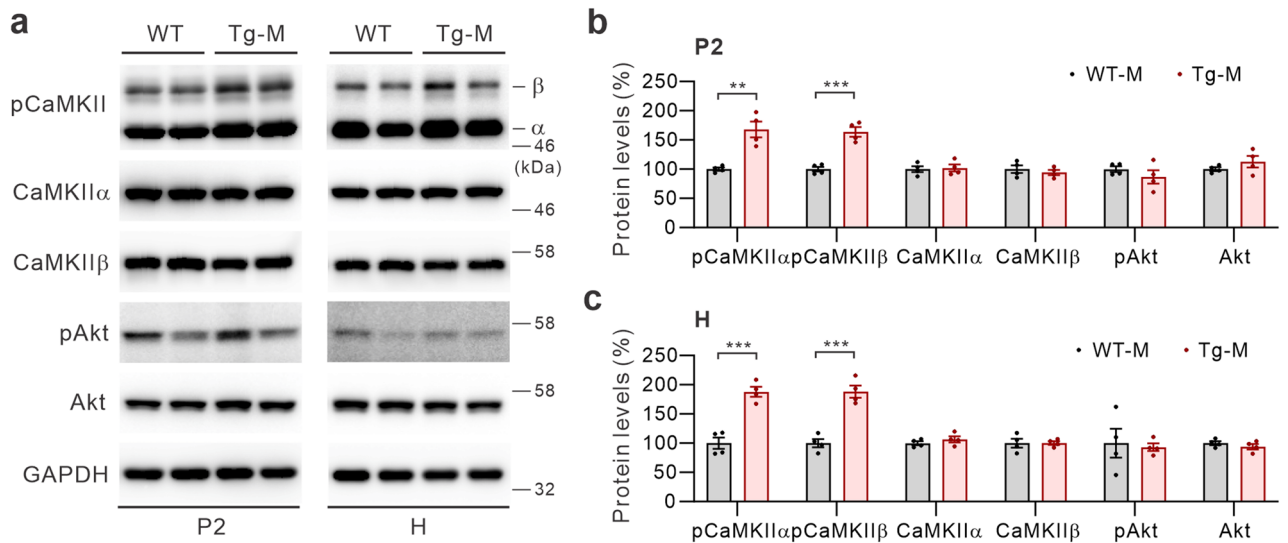


**Figure 2.** Enhanced CaMKII activity, not Akt, is associated with the hyper-phosphorylation of GSK3 $\beta$  in male S-SCAM Tg mice. **(a)** Representative immunoblots showing pCaMKIIs, CaMKII $\alpha$ , CaMKII $\beta$ , pAkt, and Akt protein levels in the P2 (left) and H fractions (right) of male S-SCAM Tg mice. **(b-c)** Quantification of P2 **(b)** and H data **(c)**.  $n = 4$  mice per group. \*\*\* $p < 0.001$ , \*\* $p < 0.01$ , unpaired  $t$ -test.

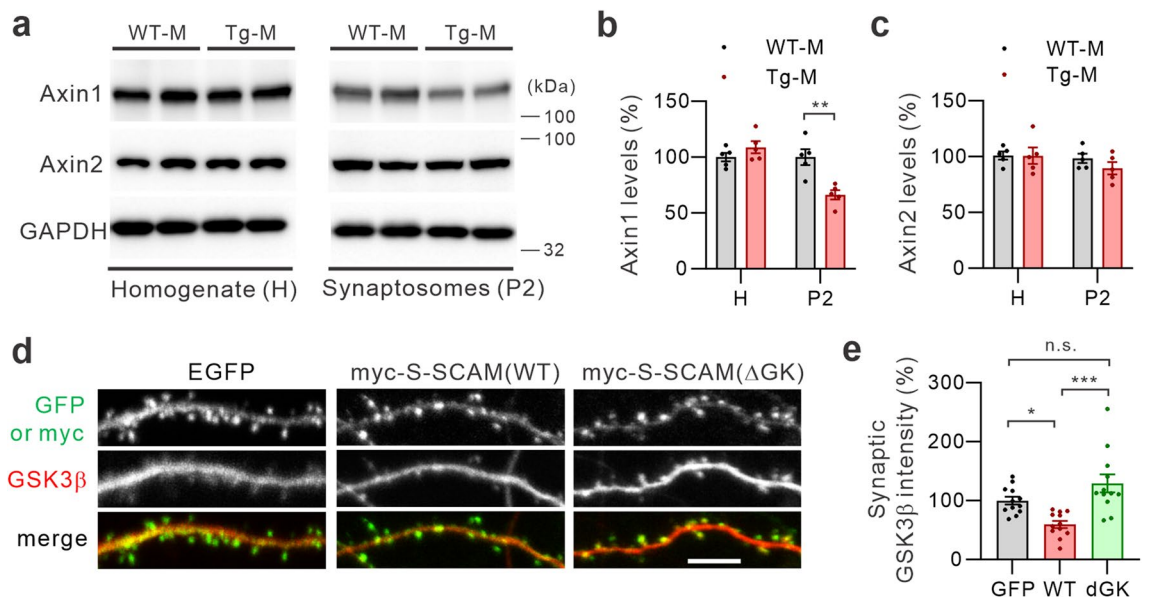


**Figure 3.** Altered synaptic Axin1 levels are responsible for the reduction of synaptic GSK3 $\beta$ . **(a-c)** Reduced Axin1 levels in the P2 fraction of male S-SCAM Tg mice. Representative immunoblots **(a)**, quantification of Axin1 **(b)** and Axin2 protein levels **(c)**.  $n = 5$  mice per group. \*\* $p < 0.01$ , unpaired  $t$ -test with Welch's correction. **(d, e)** Removal of the GK domain in S-SCAM prevents the loss of synaptic GSK3 $\beta$  in cultured hippocampal neurons. Representative images **(d)** and quantification of synaptic GSK3 $\beta$  immunofluorescent intensity **(e)**.  $n = 12$  neurons per group. One-way ANOVA,  $F_{(2,33)} = 11.62$ ,  $p < 0.001$ . Tukey's multiple comparison test: \*\*\* $p < 0.001$ , \* $p < 0.05$ . Scale bars represent 5  $\mu$ m.

NMDA treatment, we next examined the changes of GSK3 $\beta$  activity during chem-LTD in S-SCAM overexpressing neurons. Surprisingly, pS9-GSK3 $\beta$  levels were not significantly changed upon NMDA treatment in S-SCAM overexpressing neurons, indicating dysregulated GSK3 $\beta$  activity. Remarkably, XAV939 restored the temporal activation of GSK3 $\beta$  in S-SCAM overexpressing neurons, which is indistinguishable from XAV939-treated GFP control neurons (Fig. 4f, g). These results collectively suggest that S-SCAM overexpression hampers the temporal regulation of GSK3 $\beta$  activity and blocks LTD formation by inducing Axin1 deficits at synapses.

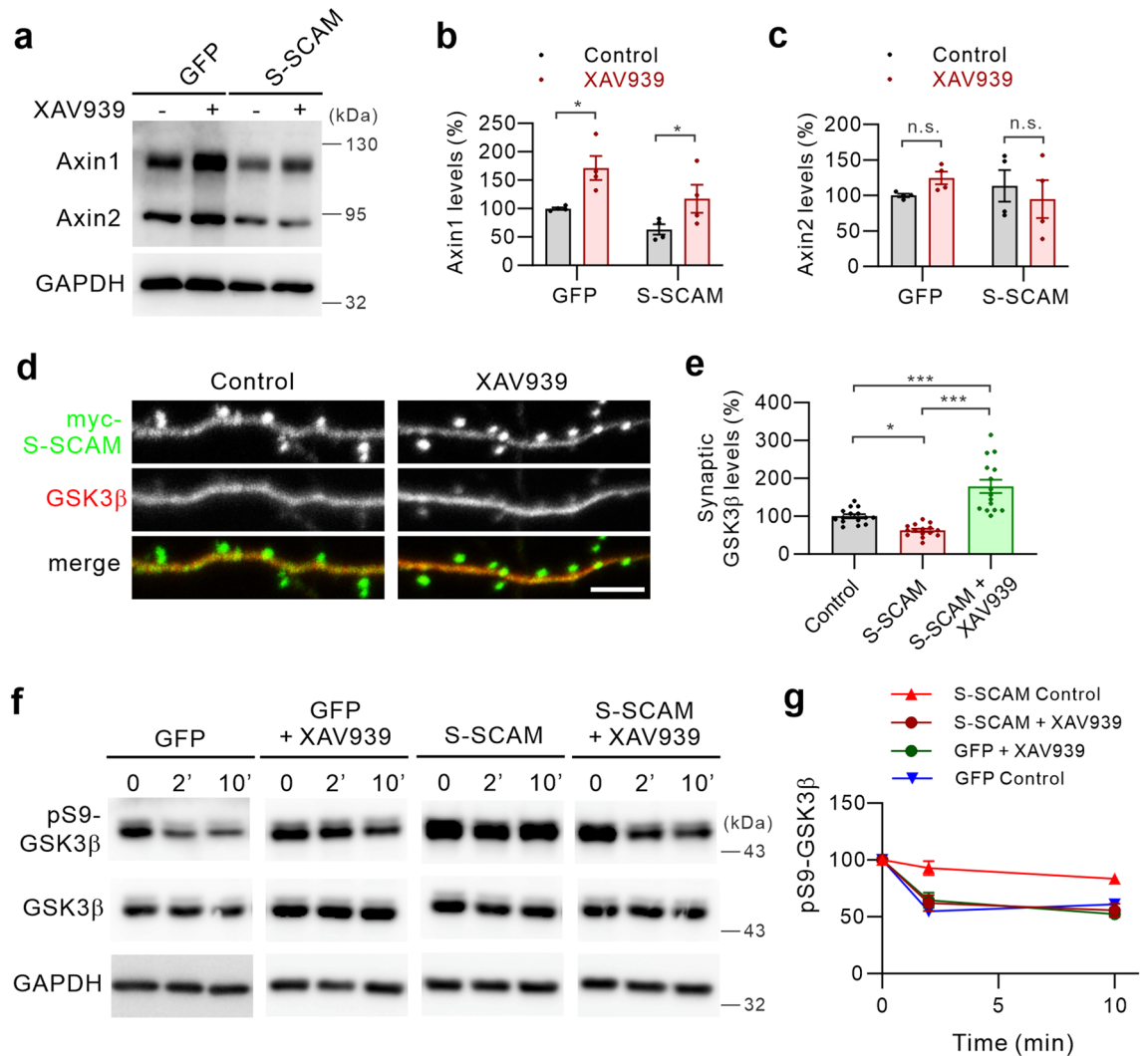


**Figure 4.** Axin stabilization restores synaptic GSK3 $\beta$  levels and its temporal regulation during Chem-LTD. (a–c) Effect of XAV939 (5 mM) on the total protein levels of Axin1 and Axin2 in GFP- or S-SCAM-overexpressing cultured hippocampal neurons. Representative immunoblots (a), and quantification of the data for Axin1 (b) and Axin2 (c).  $n = 4$  per group. \* $p < 0.05$ , unpaired  $t$ -test. (d, e) Effect of XAV939 on synaptic GSK3 $\beta$  levels in myc-S-SCAM overexpressing neurons. Representative images (d), and quantification of the data (e).  $n = 15$  per group. One-way ANOVA,  $F_{(2,42)} = 29.91$ ,  $p < 0.001$ . Tukey's multiple comparison test: \*\*\* $p < 0.0001$ , \* $p < 0.05$ . (f–g) Effect of XAV939 on the GSK3 $\beta$  activation during Chem-LTD. Representative immunoblots (f) and quantification of the data (g).  $n = 3$  per group. \* $p < 0.05$ , unpaired  $t$ -test with Welch's correction.

**17 $\beta$ -Estradiol (E2) increases Axin2 expression and preserves synaptic GSK3 $\beta$  protein levels.** To understand the male-specific deficits in synaptic plasticity in S-SCAM Tg mice, we examined whether female S-SCAM Tg mice have alterations in GSK3 $\beta$  and Axin protein levels in the P2 fractions. Unlike male Tg mice, female Tg mice do not show alterations in synaptic GSK3 $\beta$  (Fig. 5a, b) and Axin1 protein levels (Fig. 5c, d). Surprisingly, synaptic Axin2 protein levels were significantly increased in the female Tg mice ( $154\% \pm 7\%$  of WT; Fig. 5c, d). These results suggest that female-specific alteration in Axin2 may have a protective effect in preserving synaptic GSK3 $\beta$  function.

Axin2, while functionally similar to Axin1, shows distinguished expression patterns from Axin1<sup>23</sup>. For example, it was shown that Axin2 expression is inducible by Wnt signaling<sup>34,35</sup>. To investigate the effect of female sex hormone E2 on Axin2, we treated cultured hippocampal neurons with E2 (100 nM) and examined its effect on total Axin protein levels. As shown in Fig. 5e, E2 significantly increased the amount of Axin2 protein ( $149\% \pm 13\%$  of control; Fig. 5f), while Axin1 protein levels were not affected much (Fig. 5g). This E2-induced Axin2 protein increase was blocked by the transcription inhibitor actinomycin D (ActD, 2 mM; Fig. 5e, f), suggesting that E2 induces Axin2 expression. Notably, Axin1 protein levels were decreased by ActD ( $61.5\% \pm 13\%$  of control; Fig. 5g), although the data did not reach statistical significance ( $p = 0.051$ ).

Since Axin stabilization increases synaptic GSK3 $\beta$  protein levels in S-SCAM-overexpressing neurons (Fig. 4e), we next examined the effect of E2 on synaptic GSK3 $\beta$  protein levels in S-SCAM overexpressing neurons. Compared to control neurons, E2-treated neurons showed a great increase in synaptic GSK3 $\beta$  staining intensities

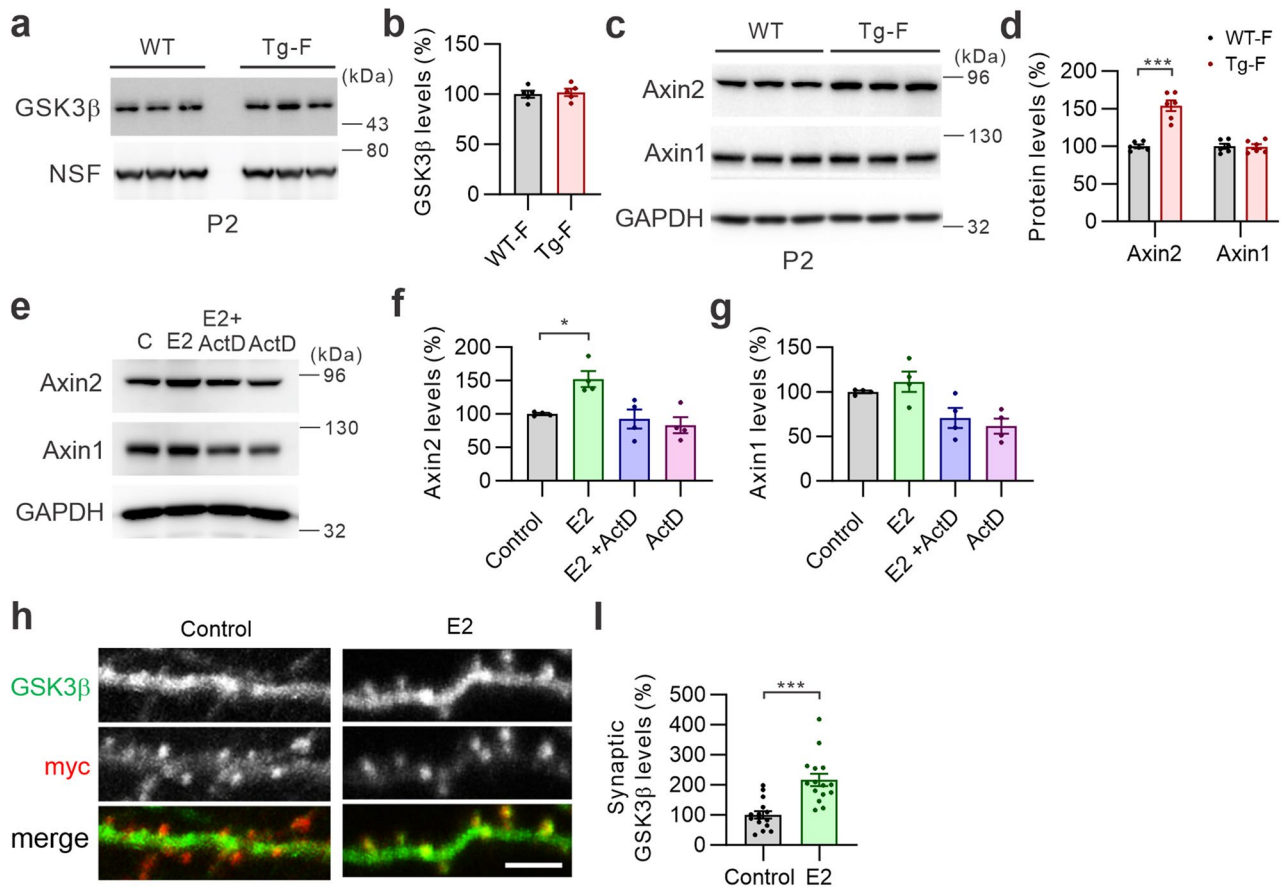


**Figure 5.** Sex-specific reduction of synaptic GSK3 $\beta$  is mediated by estradiol-mediated increase of Axin2. (a, b) Female S-SCAM Tg mice have normal synaptosomal GSK3 $\beta$  protein levels. Representative images (a) and quantification of GSK3 $\beta$  levels in the P2 fraction (b).  $n = 5$  per group. (c, d) Increased Axin2 protein levels in the P2 fraction of female S-SCAM Tg mice. Representative images (c) and quantification of Axin1 and Axin2 levels in the P2 fraction (d).  $n = 6$  per group.  $***p < 0.0001$ , unpaired  $t$ -test with Welch's correction. (e–g) E2 (10 nM) increases Axin2 protein levels in cultured hippocampal neurons. Representative images (e) and quantification of Axin1 (f) and Axin2 levels (g).  $n = 4$  per group. One-way ANOVA,  $F_{(3,12)} = 7.856$ ,  $p < 0.01$ . Tukey's multiple comparison test:  $*p < 0.05$ . (h, i) Effect of E2 on synaptic GSK3 $\beta$  levels in myc-S-SCAM overexpressing neurons. Representative images (h) and quantification of the data (i).  $n = 15$  per group.  $***p < 0.001$ , unpaired  $t$ -test with Welch's correction.

( $217\% \pm 21\%$ ; Fig. 5h, i). E2 did not have significant effect on synaptic GSK3 $\beta$  levels in GFP-transfected neurons (Supplemental Fig. 2). These results suggest that E2 preserves synaptic GSK3 $\beta$  function by increasing Axin2 expression in female Tg mice.

**S-SCAM overexpression did not change the amount of  $\beta$ -catenin.** Axin is considered as a key limiting factor for canonical Wnt signaling since it controls  $\beta$ -catenin levels by promoting the assembly of  $\beta$ -catenin destruction complex. In neurons, however,  $\beta$ -catenin also plays a structural function at synapses, independent of its role in the transcriptional regulation of Wnt signaling<sup>26</sup>. To evaluate the effect of S-SCAM overexpression on these processes, we examined the total and synaptic  $\beta$ -catenin levels in male S-SCAM Tg mice. We found that both total (H) and synaptic (P2) amounts of  $\beta$ -catenin were not significantly changed (Fig. 6a–c). Therefore, the reduction in synaptic Axin1 amounts did not cause  $\beta$ -catenin stabilization in the Tg mice. These results suggest that synaptic Axin1 plays a role in GSK3 $\beta$  recruitment and S-SCAM overexpression does not directly affect the canonical Wnt signaling.

## Discussion

In this paper, we described the intriguing interplay of S-SCAM and Axins in the assembly of the GSK3 $\beta$  signaling complex at synapses. We also uncovered the role of Axins in the sex differences displayed in S-SCAM Tg mouse model of SCZ.

There are three main findings: First, we showed that Axin plays a pivotal role in the synaptic localization of GSK3 $\beta$  and the proper assembly of the GSK3 $\beta$  signaling complex involved in synaptic plasticity. S-SCAM inhibits these processes by binding to Axin in competition with GSK3 $\beta$ . Notably, Axin mediates the synaptic localization of GSK3 $\beta$  in a manner independent of the canonical Wnt signaling, which is reminiscent of Axin's

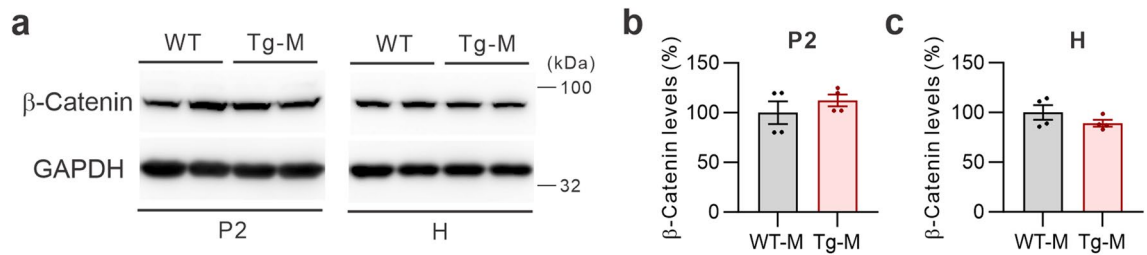


**Figure 6.** Total and synaptic  $\beta$ -catenin protein levels in S-SCAM male Tg mice. (a) Representative immunoblots showing  $\beta$ -catenin and GAPDH protein levels in the P2 (left) and H fractions (right) of male S-SCAM Tg mice. (b, c) Quantification of P2 (b) and H data (c).  $n = 4$  mice per group.

role in the axonal localization of GSK3 $\beta$ <sup>25</sup>. At this point, the molecular mechanism(s) responsible for the reduced Axin protein levels at synapses in S-SCAM overexpressing neurons remains unidentified. However, we suspect that increased glutamatergic activity at synapses might contribute to the reduction of synaptic Axin1 levels. S-SCAM Tg mice showed impaired synaptic GSK3 $\beta$  activity (shown by both reduced GSK3 $\beta$  protein levels and increased inhibitory phosphorylation), which is associated with increased CaMKII activity at synapses. Reduced GSK3 $\beta$  activity could lead to Axin reduction, since GSK3 $\beta$  stabilizes Axin via direct phosphorylation<sup>36,37</sup> and dephosphorylated Axin is degraded<sup>38,39</sup>. Moreover, it is well known that increased glutamatergic activity promotes poly-ubiquitination of synaptic proteins<sup>40,41</sup>. Axin is a target for poly-ubiquitination and subsequent degradation by proteasomes<sup>29</sup>. Interestingly, under our experimental conditions, XAV939 did not increase Axin2 levels, unlike Axin1. In addition to preventing Axin degradation, XAV939 blocks the mRNA expression of Axin2 but not Axin1<sup>23,42</sup>. Therefore, it is plausible that Axin2 protein levels did not change by XAV939 because there is no new Axin2 protein synthesis to increase total Axin2 levels. Further studies await to verify this possibility.

Second, we demonstrated that GSK3 $\beta$  hypofunction is associated with the S-SCAM Tg mouse model. GSK3 $\beta$  is a key protein kinase strongly implicated in the pathogenesis of SCZ<sup>43,44</sup>. GSK3 hyperfunction is found in individuals with SCZ<sup>45</sup>. Consistently, genetic and molecular studies confirmed the key contribution of GSK3 $\beta$  hyperfunction in the pathogenesis of SCZ<sup>44,46,47</sup>. Paradoxically, hypofunction of GSK3 $\beta$  is found in patients with SCZ. Postmortem studies of SCZ patients revealed low GSK3 $\beta$  activity<sup>48</sup>, reduced protein levels<sup>49,50</sup> (but see also<sup>51</sup>), and immunoreactivity<sup>52</sup>. Moreover, genetic association studies uncovered a single-nucleotide polymorphism that reduces GSK3 $\beta$  mRNA and protein levels in human subjects<sup>53</sup>. However, due to small sample sizes and high variability of the data, the pathophysiological significance of GSK3 $\beta$  hypofunction has remained unclear. To our knowledge, our studies provide the first preclinical evidence supporting the causal relationship of GSK3 $\beta$  hypofunction and the pathogenesis of SCZ.

Third, we identified mechanisms responsible for sex differences observed in S-SCAM Tg mice, which might be potentially relevant to SCZ. Sex differences are well documented in the humans with SCZ, which include disease risk, course, and outcome<sup>15</sup>. Men have 1.4-fold higher incidence of SCZ, display more severe symptoms and worse cognitive impairments, and are generally less responsive to antipsychotic treatments when compared to women<sup>54</sup>. Moreover, SCZ incidence in women greatly increases around menopause<sup>55</sup>. Based on sex differences of SCZ, the “estrogen hypothesis” was proposed in which the powerful female sex hormone estrogen plays a protective role against the development and severity of the disease. In clinical trials, supplemental estrogen treatment administered in conjunction with antipsychotics is beneficial for SCZ<sup>55</sup>. Our results suggest that Axin deficits at synapses are responsible for the male-specific GSK3 $\beta$  hypofunction in S-SCAM Tg mice. In female S-SCAM Tg mice, estrogen seems to buffer the Axin deficit at synapses by increasing Axin2 expression in neurons. Remarkably, Axin2 levels are increased to a level comparable to the elevated amounts of synaptic S-SCAM proteins (~1.5-fold)<sup>14</sup>. Therefore, the increase in Axin proteins seems sufficient to compensate for the increased S-SCAM levels and maintains GSK3 $\beta$  levels at synapses. These results are consistent with previous findings that, unlike Axin1, Axin2 shows an inducible expression pattern that is dependent on  $\beta$ -catenin/Tcf<sup>34</sup>. Moreover, it was shown that E2 activates  $\beta$ -catenin-dependent transcription in neurons<sup>56</sup>. Therefore, it is highly conceivable that E2 protects Axin levels at synapses in female S-SCAM Tg mice (and thereby GSK3 $\beta$  signaling complex) by promoting Axin2 transcription. Overall, our findings provide strong support for the estrogen hypothesis.

The S-SCAM Tg mice were generated by using the CaMKII promoter to drive the expression of S-SCAM transgene. Therefore, the Tg mice have elevated S-SCAM levels primarily in excitatory neurons of the forebrain area and most highly in the hippocampus<sup>57</sup>. Therefore, the sex differences observed in the Tg mice are likely caused by the excitation/inhibition imbalances in these principal neurons. Consistently, it is well documented that hippocampal functions are highly influenced by estrogen<sup>58–60</sup>. However, it remains to be determined whether sex differences of SCZ are also driven by the alterations of the glutamatergic function in the hippocampus and/or other brain regions.

We used cultured rat hippocampal neurons, which are reliable and amenable for molecular-genetic and pharmacological manipulations. These advantages allowed us to perform initial studies on the molecular mechanisms underlying sex-differences in S-SCAM Tg mice. We do not expect significant differences in rat vs mouse hippocampal neurons, since the major phenotypes of S-SCAM overexpression found from rat neurons were replicated in mouse neurons *in vivo*<sup>1,14</sup>. Further studies using the S-SCAM Tg mouse model will strengthen the role of Axin and E2 in sex-differences found in this study.

Finally, our studies provide a potential new therapeutic target for SCZ. Recent reports demonstrated that chronic intraperitoneal XAV939 treatment of mice has an impact on the Wnt signaling in the brains, suggesting

that XAV939 passes the blood–brain barrier and stabilizes Axin<sup>61</sup>. Therefore it would be interesting to investigate the effect of XAV939 on the SCZ-like behavioral deficits displayed in S-SCAM male Tg mice, especially on synaptic plasticity and working memory deficits.

## Methods

**Animals.** S-SCAM Tg mice (C57BL/6J-Tg(Camk2a-Magi2)1Shlee/J; Jackson stock No: 027306) were maintained as described<sup>14</sup>. Timed pregnant Sprague-Dawley female rats were obtained from Envigo. All experimental procedures involving the mice and rats were performed in accordance with the relevant guidelines and regulations and approved by the Institutional Animal Care and Use Committee in the Medical College of Wisconsin. All methods are reported in accordance with ARRIVE guidelines.

**Cultured rat hippocampal neurons and transfection.** Dissociated rat hippocampal neuron culture was prepared from E18 embryos (both sexes were used) of Sprague Dawley rats and maintained in Neurobasal medium supplemented with B27 and Pen/Strep (ThermoFisher Scientific) as described previously<sup>62</sup>. Hippocampal neurons were transfected at div14 using Lipofectamine 2000 as described previously<sup>63</sup>.

**Reagents.** XAV939 and  $\beta$ -estradiol (E2) were purchased from Tocris. Actinomycin D was obtained from Sigma.

**Immunocytochemistry.** Transfected neurons were fixed at 2 days post-transfection. Immunocytochemistry was performed as described<sup>1,63</sup>. Briefly, hippocampal neurons were first fixed in 4% formaldehyde/1  $\times$  PBS/4% sucrose for 15 min followed by membrane permeabilization in 0.5% TritonX-100/1  $\times$  PBS for 10 min. After washing three times in 1  $\times$  PBS for 10 min, fixed neurons were incubated with primary antibodies diluted in 1  $\times$  GDB (0.1% gelatin, 0.3% Triton X-100, 0.45 M NaCl, 17.7 mM sodium phosphate buffer, pH 7.4) in a humidified chamber overnight at 4  $^{\circ}$ C. Primary antibodies used and their dilution factors are: rabbit anti-GSK3 $\beta$  (1:100; Abcam), rat anti-HA (1:250; Roche), or mouse anti-myc antibodies (1:100; Santa Cruz Biotechnology). Bound primary antibodies were detected using Alexa 488-(ThermoFisher) or Cy3-conjugated secondary antibodies (Jackson ImmunoResearch Laboratories).

**Immunocytochemical image acquisition and analyses.** Images were acquired by using a Nikon CI plus laser scanning confocal microscope and 60 $\times$  objective (NA1.4). Acquired images (z-series stacks) were first converted to projection images (with maximal projection option) for analyses. Both image acquisition and analyses were done in a blind manner. To measure synaptic GSK3 $\beta$  intensities, 15–30 dendritic spine regions were randomly selected from the dendrites of transfected neurons based on GFP or myc fluorescence (overexpressed S-SCAM is highly enriched in dendritic spines<sup>1</sup>) using SynPAnal software<sup>64</sup>. After applying threshold, integrated intensity values from individual spines were obtained and average values of them were calculated per neuron basis in Excel. All data were transferred to GraphPad Prism software for computation and graphical representation.

**Western blotting analyses.** Total homogenate (H) and synaptosome (P2) fractions of mouse forebrain tissues were prepared as described before<sup>27</sup>. For the preparation of TCL from cultured neurons, pre-heated 2 $\times$  SDS sample buffer (65  $^{\circ}$ C) was directly added to the wells of culture dishes after washing once in ice-cold 1  $\times$  PBS. The H fractions, P2 fractions, or TCLs were separated on SDS–polyacrylamide gels and transferred onto PVDF membrane (Immobilon-P; Millipore). The membrane was blocked in 6% nonfat-dried milk/1  $\times$  TBS-T. Primary antibodies used in the studies are: mouse anti-GSK3 $\beta$  (1:1000; Cell Signaling Technology), rabbit anti-phospho-GSK3 $\beta$  (Ser9; 1:1000; Cell Signaling Technology), rabbit anti-GAPDH (1:1000; Cell Signaling Technology), rabbit anti-Axin1 (1:1000; Cell Signaling Technology), mouse anti- $\beta$ -catenin (1:500; Millipore), mouse anti-CaMKIIa (1:100; ThermoFisher Scientific), mouse anti-CaMKIIb (1:1000; ThermoFisher Scientific), rabbit anti-phospho-CaMKII (Thr286; 1:1000; Phospho Solutions), rabbit anti-Akt (1:1000; Cell Signaling Technology), rabbit anti-phospho Akt (Thr308; 1:1000; Cell Signaling Technology), rabbit anti-Axin2 (1:1000; Abcam), and mouse anti-NSF (1:2000; Millipore). Primary antibodies were diluted in the blocking buffer and incubated overnight at 4  $^{\circ}$ C. After washing in 1  $\times$  TBS-T, membranes were further incubated for 1 h with HRP-conjugated secondary antibodies (GE Healthcare or Cytiva). Bound antibodies were detected by using SuperSignal West Pico Plus Chemiluminescent substrates (Thermo Scientific) and images were acquired by using luminescent image analyzer (ImageQuant LAS4000, GE Healthcare).

**Statistical analyses.** All neuron experiments were performed at least in triplicate using independent batches of hippocampal neuron cultures. All data values represent means  $\pm$  s.e.m. For multiple group comparisons, one-way ANOVA with Tukey's multiple comparison post hoc test were performed using the GraphPad Prism software. Welch's t test (unpaired) was used to determine the statistical significance for two groups.  $p < 0.05$  was considered significant.

## Data availability

All materials, data, and associated protocols will be promptly made available to readers without undue qualifications in material transfer agreements.

Received: 6 August 2021; Accepted: 4 March 2022

Published online: 08 March 2022

## References

- Danielson, E. *et al.* S-SCAM/MAGI-2 is an essential synaptic scaffolding molecule for the GluA2-containing maintenance pool of AMPA receptors. *J. Neurosci. Off. J. Soc. Neurosci.* **32**, 6967–6980. <https://doi.org/10.1523/JNEUROSCI.0025-12.2012> (2012).
- Hirao, K. *et al.* A novel multiple PDZ domain-containing molecule interacting with N-methyl-D-aspartate receptors and neuronal cell adhesion proteins. *J. Biol. Chem.* **273**, 21105–21110 (1998).
- Ihara, K. I., Nishimura, T., Fukuda, T., Ookura, T. & Nishimori, K. Generation of Venus reporter knock-in mice revealed MAGI-2 expression patterns in adult mice. *Gene Expr. Patterns GEP* <https://doi.org/10.1016/j.gep.2012.01.006> (2012).
- Sumita, K. *et al.* Synaptic scaffolding molecule (S-SCAM) membrane-associated guanylate kinase with inverted organization (MAGI)-2 is associated with cell adhesion molecules at inhibitory synapses in rat hippocampal neurons. *J. Neurochem.* **100**, 154–166. <https://doi.org/10.1111/j.1471-4159.2006.04170.x> (2007).
- Danielson, E., Metallo, J. & Lee, S. H. Role of TARP interaction in S-SCAM-mediated regulation of AMPA receptors. *Channels (Austin)* **6**, 393–397 (2012).
- Nagashima, S., Kodaka, M., Iwasa, H. & Hata, Y. MAGI2/S-SCAM outside brain. *J. Biochem.* **157**, 177–184. <https://doi.org/10.1093/jb/mvv009> (2015).
- Hirabayashi, S. *et al.* Synaptic scaffolding molecule interacts with axin. *J. Neurochem.* **90**, 332–339. <https://doi.org/10.1111/j.1471-4159.2004.02497.x> (2004).
- Deng, F., Price, M. G., Davis, C. F., Mori, M. & Burgess, D. L. Stargazin and other transmembrane AMPA receptor regulating proteins interact with synaptic scaffolding protein MAGI-2 in brain. *J. Neurosci. Off. J. Soc. Neurosci.* **26**, 7875–7884. <https://doi.org/10.1523/JNEUROSCI.1851-06.2006> (2006).
- Walsh, T. *et al.* Rare structural variants disrupt multiple genes in neurodevelopmental pathways in schizophrenia. *Science* **320**, 539–543. <https://doi.org/10.1126/science.1155174> (2008).
- Karlsson, R. *et al.* MAGI1 copy number variation in bipolar affective disorder and schizophrenia. *Biol. Psychiatry* **71**, 922–930. <https://doi.org/10.1016/j.biopsych.2012.01.020> (2012).
- Koide, T. *et al.* Common variants in MAGI2 gene are associated with increased risk for cognitive impairment in schizophrenic patients. *PLoS ONE* **7**, e36836. <https://doi.org/10.1371/journal.pone.0036836> (2012).
- Buxbaum, J. D. *et al.* Molecular dissection of NRG1-ERBB4 signaling implicates PTPRZ1 as a potential schizophrenia susceptibility gene. *Mol. Psychiatry* **13**, 162–172. <https://doi.org/10.1038/sj.mp.4001991> (2008).
- Shin, S. M., Skaar, S., Danielson, E. & Lee, S. H. Aberrant expression of S-SCAM causes the loss of GABAergic synapses in hippocampal neurons. *Sci. Rep.* **10**, 83. <https://doi.org/10.1038/s41598-019-57053-y> (2020).
- Zhang, N. *et al.* S-SCAM, a rare copy number variation gene, induces schizophrenia-related endophenotypes in transgenic mouse model. *J. Neurosci. Off. J. Soc. Neurosci.* **35**, 1892–1904. <https://doi.org/10.1523/JNEUROSCI.3658-14.2015> (2015).
- Abel, K. M., Drake, R. & Goldstein, J. M. Sex differences in schizophrenia. *Int. Rev. Psychiatry* **22**, 417–428. <https://doi.org/10.3109/09540261.2010.515205> (2010).
- Hooper, C. *et al.* Glycogen synthase kinase-3 inhibition is integral to long-term potentiation. *Eur. J. Neurosci.* **25**, 81–86. <https://doi.org/10.1111/j.1460-9568.2006.05245.x> (2007).
- Peineau, S. *et al.* LTP inhibits LTD in the hippocampus via regulation of GSK3beta. *Neuron* **53**, 703–717. <https://doi.org/10.1016/j.neuron.2007.01.029> (2007).
- Zhu, L. Q. *et al.* Activation of glycogen synthase kinase-3 inhibits long-term potentiation with synapse-associated impairments. *J. Neurosci. Off. J. Soc. Neurosci.* **27**, 12211–12220. <https://doi.org/10.1523/JNEUROSCI.3321-07.2007> (2007).
- Peineau, S. *et al.* The role of GSK-3 in synaptic plasticity. *Br. J. Pharmacol.* **153**(Suppl 1), S428–437. <https://doi.org/10.1038/bjp.2008.2> (2008).
- Hur, E. M. & Zhou, F. Q. GSK3 signalling in neural development. *Nat. Rev. Neurosci.* **11**, 539–551. <https://doi.org/10.1038/nrn2870> (2010).
- Nelson, C. D., Kim, M. J., Hsin, H., Chen, Y. & Sheng, M. Phosphorylation of threonine-19 of PSD-95 by GSK-3beta is required for PSD-95 mobilization and long-term depression. *J. Neurosci. Off. J. Soc. Neurosci.* **33**, 12122–12135. <https://doi.org/10.1523/JNEUROSCI.0131-13.2013> (2013).
- Li, V. S. *et al.* Wnt signaling through inhibition of beta-catenin degradation in an intact Axin1 complex. *Cell* **149**, 1245–1256. <https://doi.org/10.1016/j.cell.2012.05.002> (2012).
- Mazzoni, S. M. & Fearon, E. R. AXIN1 and AXIN2 variants in gastrointestinal cancers. *Cancer Lett.* **355**, 1–8. <https://doi.org/10.1016/j.canlet.2014.09.018> (2014).
- Chen, Y. *et al.* Axin regulates dendritic spine morphogenesis through Cdc42-dependent signaling. *PLoS ONE* **10**, e0133115. <https://doi.org/10.1371/journal.pone.0133115> (2015).
- Fang, W. Q. *et al.* Cdk5-mediated phosphorylation of Axin directs axon formation during cerebral cortex development. *J. Neurosci. Off. J. Soc. Neurosci.* **31**, 13613–13624. <https://doi.org/10.1523/JNEUROSCI.3120-11.2011> (2011).
- Chen, Y., Fu, A. K. & Ip, N. Y. Axin: An emerging key scaffold at the synapse. *IUBMB Life* **65**, 685–691. <https://doi.org/10.1002/iub.1184> (2013).
- Lee, S. H., Valtschanoff, J. G., Kharazia, V. N., Weinberg, R. & Sheng, M. Biochemical and morphological characterization of an intracellular membrane compartment containing AMPA receptors. *Neuropharmacology* **41**, 680–692 (2001).
- Song, B. *et al.* Inhibitory phosphorylation of GSK-3 by CaMKII couples depolarization to neuronal survival. *J. Biol. Chem.* **285**, 41122–41134. <https://doi.org/10.1074/jbc.M110.130351> (2010).
- Song, X., Wang, S. & Li, L. New insights into the regulation of Axin function in canonical Wnt signaling pathway. *Protein Cell* **5**, 186–193. <https://doi.org/10.1007/s13238-014-0019-2> (2014).
- Huang, S. M. *et al.* Tankyrase inhibition stabilizes axin and antagonizes Wnt signalling. *Nature* **461**, 614–620. <https://doi.org/10.1038/nature08356> (2009).
- Narwal, M. *et al.* Discovery of tankyrase inhibiting flavones with increased potency and isoenzyme selectivity. *J. Med. Chem.* **56**, 7880–7889. <https://doi.org/10.1021/jm401463y> (2013).
- Lee, H. K., Kameyama, K., Huganir, R. L. & Bear, M. F. NMDA induces long-term synaptic depression and dephosphorylation of the GluR1 subunit of AMPA receptors in hippocampus. *Neuron* **21**, 1151–1162 (1998).
- Cymerman, I. A. *et al.* Structural plasticity of dendritic spines requires GSK3alpha and GSK3beta. *PLoS ONE* **10**, e0134018. <https://doi.org/10.1371/journal.pone.0134018> (2015).
- Leung, J. Y. *et al.* Activation of AXIN2 expression by beta-catenin-T cell factor. A feedback repressor pathway regulating Wnt signaling. *J. Biol. Chem.* **277**, 21657–21665. <https://doi.org/10.1074/jbc.M200139200> (2002).
- Lustig, B. *et al.* Negative feedback loop of Wnt signaling through upregulation of conductin/axin2 in colorectal and liver tumors. *Mol. Cell. Biol.* **22**, 1184–1193 (2002).
- Yamamoto, H. *et al.* Phosphorylation of axin, a Wnt signal negative regulator, by glycogen synthase kinase-3beta regulates its stability. *J. Biol. Chem.* **274**, 10681–10684 (1999).

37. Jho, E., Lomvardas, S. & Costantini, F. A GSK3beta phosphorylation site in axin modulates interaction with beta-catenin and Tcf-mediated gene expression. *Biochem. Biophys. Res. Commun.* **266**, 28–35. <https://doi.org/10.1006/bbrc.1999.1760> (1999).
38. Strovel, E. T., Wu, D. & Sussman, D. J. Protein phosphatase 2Calpha dephosphorylates axin and activates LEF-1-dependent transcription. *J. Biol. Chem.* **275**, 2399–2403. <https://doi.org/10.1074/jbc.275.4.2399> (2000).
39. Willert, K., Shibamoto, S. & Nusse, R. Wnt-induced dephosphorylation of axin releases beta-catenin from the axin complex. *Genes Dev.* **13**, 1768–1773. <https://doi.org/10.1101/gad.13.14.1768> (1999).
40. Ehlers, M. D. Activity level controls postsynaptic composition and signaling via the ubiquitin-proteasome system. *Nat. Neurosci.* **6**, 231–242. <https://doi.org/10.1038/nn1013> (2003).
41. Shin, S. M. *et al.* GKAP orchestrates activity-dependent postsynaptic protein remodeling and homeostatic scaling. *Nat. Neurosci.* **15**, 1655–1666. <https://doi.org/10.1038/nn.3259> (2012).
42. Fancy, S. P. *et al.* Axin2 as regulatory and therapeutic target in newborn brain injury and remyelination. *Nat. Neurosci.* **14**, 1009–1016. <https://doi.org/10.1038/nn.2855> (2011).
43. Lovestone, S., Killick, R., Di Forti, M. & Murray, R. Schizophrenia as a GSK-3 dysregulation disorder. *Trends Neurosci.* **30**, 142–149. <https://doi.org/10.1016/j.tins.2007.02.002> (2007).
44. Emamian, E. S. AKT/GSK3 signaling pathway and schizophrenia. *Front. Mol. Neurosci.* **5**, 33. <https://doi.org/10.3389/fnmol.2012.00033> (2012).
45. Emamian, E. S., Hall, D., Birnbaum, M. J., Karayiorgou, M. & Gogos, J. A. Convergent evidence for impaired AKT1-GSK3beta signaling in schizophrenia. *Nat. Genet.* **36**, 131–137. <https://doi.org/10.1038/ng1296> (2004).
46. Mao, Y. *et al.* Disrupted in schizophrenia 1 regulates neuronal progenitor proliferation via modulation of GSK3beta/beta-catenin signaling. *Cell* **136**, 1017–1031. <https://doi.org/10.1016/j.cell.2008.12.044> (2009).
47. Tamura, M., Mukai, J., Gordon, J. A. & Gogos, J. A. Developmental inhibition of Gsk3 rescues behavioral and neurophysiological deficits in a mouse model of schizophrenia predisposition. *Neuron* **89**, 1100–1109. <https://doi.org/10.1016/j.neuron.2016.01.025> (2016).
48. Kozlovsky, N., Belmaker, R. H. & Agam, G. Low GSK-3 activity in frontal cortex of schizophrenic patients. *Schizophr. Res.* **52**, 101–105 (2001).
49. Nadri, C., Dean, B., Scarr, E. & Agam, G. GSK-3 parameters in postmortem frontal cortex and hippocampus of schizophrenic patients. *Schizophr. Res.* **71**, 377–382. <https://doi.org/10.1016/j.schres.2004.02.020> (2004).
50. Beasley, C. *et al.* Glycogen synthase kinase-3beta immunoreactivity is reduced in the prefrontal cortex in schizophrenia. *Neurosci. Lett.* **302**, 117–120 (2001).
51. Beasley, C., Cotter, D. & Everall, I. An investigation of the Wnt-signalling pathway in the prefrontal cortex in schizophrenia, bipolar disorder and major depressive disorder. *Schizophr. Res.* **58**, 63–67 (2002).
52. Kozlovsky, N., Belmaker, R. H. & Agam, G. Low GSK-3beta immunoreactivity in postmortem frontal cortex of schizophrenic patients. *Am. J. Psychiatry* **157**, 831–833 (2000).
53. Blasi, G. *et al.* Association of GSK-3beta genetic variation with GSK-3beta expression, prefrontal cortical thickness, prefrontal physiology, and schizophrenia. *Am. J. Psychiatry* **170**, 868–876. <https://doi.org/10.1176/appi.ajp.2012.12070908> (2013).
54. Kulkarni, J., Hayes, E. & Gavrilidis, E. Hormones and schizophrenia. *Curr. Opin. Psychiatry* **25**, 89–95. <https://doi.org/10.1097/YCO.0b013e328350360e> (2012).
55. Mukai, J. *et al.* Molecular substrates of altered axonal growth and brain connectivity in a mouse model of schizophrenia. *Neuron* **86**, 680–695. <https://doi.org/10.1016/j.neuron.2015.04.003> (2015).
56. Varea, O. *et al.* Estradiol activates beta-catenin dependent transcription in neurons. *PLoS ONE* **4**, e15153. <https://doi.org/10.1371/journal.pone.0005153> (2009).
57. Wang, X., Zhang, C., Szabo, G. & Sun, Q. Q. Distribution of CaMKIIalpha expression in the brain in vivo, studied by CaMKIIalpha-GFP mice. *Brain Res.* **1518**, 9–25. <https://doi.org/10.1016/j.brainres.2013.04.042> (2013).
58. Walf, A. A. & Frye, C. A. A review and update of mechanisms of estrogen in the hippocampus and amygdala for anxiety and depression behavior. *Neuropsychopharmacol. Off. Publ. Am. Coll. Neuropsychopharmacol.* **31**, 1097–1111. <https://doi.org/10.1038/sj.npp.1301067> (2006).
59. Mukai, H. *et al.* Modulation of synaptic plasticity by brain estrogen in the hippocampus. *Biochem. Biophys. Acta.* **1800**, 1030–1044. <https://doi.org/10.1016/j.bbagen.2009.11.002> (2010).
60. Lu, Y. *et al.* Neuron-derived estrogen regulates synaptic plasticity and memory. *J. Neurosci. Off. J. Soc. Neurosci.* **39**, 2792–2809. <https://doi.org/10.1523/JNEUROSCI.1970-18.2019> (2019).
61. Tapia-Rojas, C. & Inestrosa, N. C. Wnt signaling loss accelerates the appearance of neuropathological hallmarks of Alzheimer's disease in J20-APP transgenic and wild-type mice. *J. Neurochem.* **144**, 443–465. <https://doi.org/10.1111/jnc.14278> (2018).
62. Kaeck, S. & Banker, G. Culturing hippocampal neurons. *Nat. Protoc.* **1**, 2406–2415. <https://doi.org/10.1038/nprot.2006.356> (2006).
63. Lee, S. H. *et al.* Reciprocal control of excitatory synapse numbers by Wnt and Wnt inhibitor PRR7 secreted on exosomes. *Nat. Commun.* **9**, 3434. <https://doi.org/10.1038/s41467-018-05858-2> (2018).
64. Danielson, E. & Lee, S. H. SynPAAnal: Software for rapid quantification of the density and intensity of protein puncta from fluorescence microscopy images of neurons. *PLoS ONE* **9**, e115298. <https://doi.org/10.1371/journal.pone.0115298> (2014).

## Acknowledgements

This research was supported by funding provided through the Research and Education Program, a component of the Advancing a Healthier Wisconsin endowment at the Medical College of Wisconsin, and NIH MH119105.

## Author contributions

S.H.L. conceived and designed the study; G.K., D.G., D.N.T., S.M.S., and S.H.L. performed experiments; S.M.S., D.N.T., and S.H.L. analyzed data; S.H.L. wrote the paper with the help of G.K. All authors reviewed the manuscript.

## Competing interests

The authors declare no competing interests.

## Additional information

**Supplementary Information** The online version contains supplementary material available at <https://doi.org/10.1038/s41598-022-08220-1>.

**Correspondence** and requests for materials should be addressed to S.H.L.

**Reprints and permissions information** is available at [www.nature.com/reprints](http://www.nature.com/reprints).

**Publisher's note** Springer Nature remains neutral with regard to jurisdictional claims in published maps and institutional affiliations.



**Open Access** This article is licensed under a Creative Commons Attribution 4.0 International License, which permits use, sharing, adaptation, distribution and reproduction in any medium or format, as long as you give appropriate credit to the original author(s) and the source, provide a link to the Creative Commons licence, and indicate if changes were made. The images or other third party material in this article are included in the article's Creative Commons licence, unless indicated otherwise in a credit line to the material. If material is not included in the article's Creative Commons licence and your intended use is not permitted by statutory regulation or exceeds the permitted use, you will need to obtain permission directly from the copyright holder. To view a copy of this licence, visit <http://creativecommons.org/licenses/by/4.0/>.

© The Author(s) 2022